RESEARCH ARTICLE | JULY 07 2025

# Polarization diagnosis and transmission distortion calibration of the Dalian coherent light source **⊘**

Mingchang Wang 0; Bingbing Zhang 0; Siyuan Tan 0; Zhixiang Wen 0; Jinxin Wang 0; Long Huang 0; Baoning Sun 0; Zequn Wang 0; Jitao Sun 0; Xinmeng Li 0; Jiayue Yang 0; Qinming Li  $\boxtimes$  0; Weiqing Zhang  $\boxtimes$  0



Rev. Sci. Instrum. 96, 073101 (2025) https://doi.org/10.1063/5.0276737





# Articles You May Be Interested In

Multi-functional gas cell in the vacuum ultraviolet free-electron laser beamline

Rev. Sci. Instrum. (June 2024)

Photodissociation dynamics of H<sub>2</sub>O at 111.5 nm by a vacuum ultraviolet free electron laser

J. Chem. Phys. (March 2018)

Quantum state-to-state vacuum ultraviolet photodissociation dynamics of small molecules

Chin. J. Chem. Phys. (February 2019)





**Published Online: 7 July 2025** 

# Polarization diagnosis and transmission distortion calibration of the Dalian coherent light source

Cite as: Rev. Sci. Instrum. 96, 073101 (2025); doi: 10.1063/5.0276737 Submitted: 20 April 2025 • Accepted: 17 June 2025 •

5 ·







Mingchang Wang,<sup>1,2</sup> Bingbing Zhang,<sup>3</sup> Siyuan Tan,<sup>1</sup> Zhixiang Wen,<sup>3</sup> Jinxin Wang,<sup>3</sup> Long Huang,<sup>3</sup> Baoning Sun,<sup>1,2</sup> Zequn Wang,<sup>4</sup> Jitao Sun,<sup>3</sup> Xinmeng Li,<sup>1,2</sup> Jiayue Yang,<sup>1</sup> Oinming Li,<sup>3,a)</sup> and Weiging Zhang<sup>1,a)</sup>

#### **AFFILIATIONS**

- <sup>1</sup> State Key Laboratory of Chemical Reaction Dynamics and Dalian Coherent Light Source, Dalian Institute of Chemical Physics, Chinese Academy of Sciences, 457 Zhongshan Road, Dalian 116023, China
- <sup>2</sup>University of Chinese Academy of Sciences, 19 A Yuquan Road, Beijing 100049, China
- Institute of Advanced Light Source Facilities, Shenzhen, 268 Zhenyuan Road, Shenzhen 518107, China
- <sup>4</sup>Dalian University of Technology, No. 2 Linggong Road, Dalian 116024, China
- a) Authors to whom correspondence should be addressed: liqinming@mail.iasf.ac.cn and weiqingzhang@dicp.ac.cn. Tel.:+86-0411-84379867

### **ABSTRACT**

Polarized light serves as a fundamental tool in various scientific research, particularly in the study of chiral molecules and magnetic materials. For Free-electron Laser (FEL) sources, the Elliptical Polarized Undulator (EPU) has been extensively used as a tool to generate tunable polarized FEL. The accurate adjustment of the polarization state critically depends on the precise diagnosis of the polarization state. This work presents a Vacuum Ultraviolet (VUV) polarimeter that employs a reflection polarizer to determine the polarization state of the Dalian Coherent Light Source (DCLS), a VUV-FEL facility in Dalian, China. This instrument has been precisely installed on the DCLS-FEL2 beamline to measure the EPU-generated FEL pulses. The linear polarization angle was measured with an accuracy of  $\pm 1^{\circ}$ , and a polarization degree of 95% was achieved at 10.2 eV photon energy. Furthermore, beamline transmission matrix calibration has been conducted to ensure precision of polarization state at downstream end-stations.

Published under an exclusive license by AIP Publishing. https://doi.org/10.1063/5.0276737

#### I. INTRODUCTION

Free-electron Lasers (FELs) exhibit high peak power, narrow bandwidth, and high coherence, making them invaluable in various research domains, including materials science, chemical engineering, and biopharmaceutics.<sup>1</sup> The Dalian Coherent Light Source (DCLS),<sup>2–4</sup> a Vacuum Ultraviolet (VUV) FEL user facility with electron beam energy of 300 MeV and a wavelength of 50–150 nm, has been serving the scientific community since its first emission at the end of 2016. At DCLS, the implementation of the Elliptical Polarized Undulator (EPU) in recent years has enabled the emission of lasers with tunable polarization states.<sup>5,6</sup> Polarized FEL provides a pivotal tool for scientific research,<sup>7–10</sup> while the polarization information is crucial for light source optimization and experimental data analysis. For instance, in atom-surface scattering experiments, it is critical to have fast and slow H atom sources with different angles

of linear polarization. <sup>11,12</sup> In the probing of low-concentration chiral samples or low-response magnetic materials, a high circular polarization degree is essential for the acquisition of experimental signals. <sup>13,14</sup> Therefore, polarization diagnostics is indispensable for the advancement of photon science.

Traditional polarization diagnostic methods primarily utilize transmissive waveplates and polarizers. These methods are only applicable to visible light and are unusable in the short wavelength range due to the lack of transmittance.<sup>15</sup> Therefore, short wavelength polarization diagnostics primarily rely on the reflection polarization technique, <sup>16,17</sup> photoelectron time-of-flight (e-TOF) spectroscopy, <sup>18,19</sup> and the fluorescence method.<sup>20</sup> The e-TOF technique, utilizing the angular distribution of photoelectrons ionized by polarized light, is a real-time, online diagnostic method. However, the accuracy and stability of the e-TOF technique are easily affected by many factors, including gas pressure, electron drift distance, and

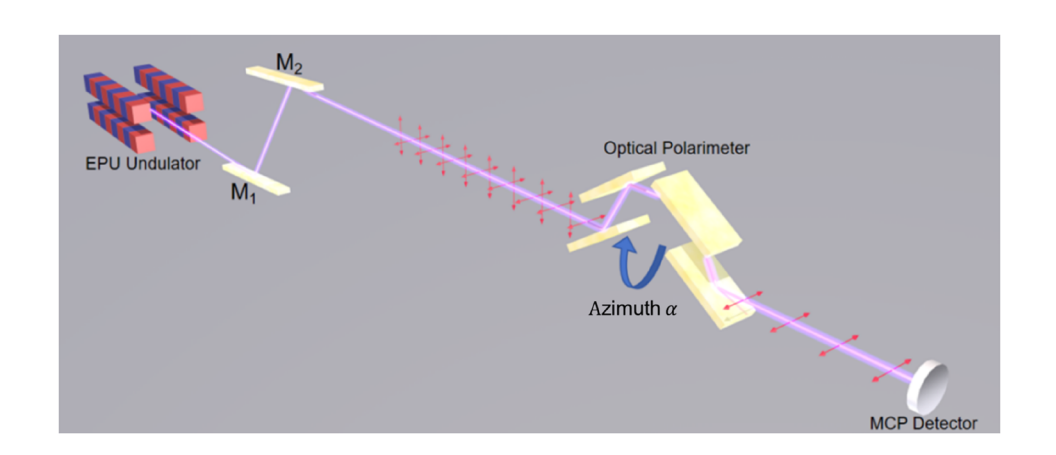


**FIG. 1.** Schematic diagram of the four-mirror polarizer of DCLS-FEL2.

residual magnetic field.<sup>21</sup> The fluorescence method employs fluorescent gases with the optical characteristics to transform ultraviolet light into visible light while maintaining the original polarization state and enabling the use of traditional polarization diagnostic methods. However, the scarcity of fluorescent gases suitable for this purpose restricts its application to the limited wavelength range, thereby reducing its versatility.

The reflection polarization technique relies on the principle of Brewster angle polarization, utilizing the difference in reflectivity between S- and P-direction polarization components to separate and detect the polarization component. The output light intensity is measured with the rotation of the polarizer along the incident direction to diagnose the polarization state of the incident light. The reflection polarization method offers high accuracy and stability, and it is suitable for the full wavelength range of DCLS as the universal technique. We use this reflection polarizer to accurately obtain the linear polarization angle, linear and circular polarization degrees, and to calibrate the beamline transmission matrix of DCLS-FEL2. It provides an important reference for the end-stations and beamline commissioning.

# II. METHODOLOGY

In the context of user experiments, the polarization state of the incident beam entering the experimental station chamber assumes paramount importance, as it serves as a critical reference point for the subsequent data processing. It is therefore situated at the extremities of the beamline and the front end of the experimental station. DCLS-FEL2 fully employs EPU, which is capable of producing radiation with tunable polarization, generating single-pulse energy up to  $100~\mu J$ , and offering two pulse duration modes ( $100~\rm fs$  and  $2~\rm ps$ ). In the beamline, there is a toroidal mirror (M1) and a plane mirror (M2). M1 is positioned 32 m from the source and focuses the beam spot in both the horizontal and vertical directions. M2 is positioned

2.5 m from M1 and is responsible for correcting the optical path tilt induced by M1. At the same time, the horizontal light offset made by the M1 and M2 combination can shield the bremsstrahlung along with FEL from upstream. The center of M2 is carved with a variable line spacing grating for online spectral diagnostics. The schematic diagram of the four-mirror polarizer and DCLS-FEL2 beamline is shown in Fig. 1.

# A. Principle of design

Stokes parameters, denoted as  $\begin{bmatrix} S_0 & S_1 & S_2 & S_3 \end{bmatrix}$ , are widely used to describe the polarization state. Parameter  $S_0$  represents the total light intensity,  $S_1$  represents the difference between the horizontal and vertical linear polarization components,  $S_2$  represents the difference between the +45° and -45° linear polarization components, and  $S_3$  represents the circular polarization component. Furthermore, the degree of linear polarization  $P_L$ , the degree of circular polarization  $P_C$ , and the polarization angle  $\theta$  can be deduced using these Stokes parameters, as shown in the following formula:

$$\begin{cases} P_{L} = \frac{\sqrt{S_{1}^{2} + S_{2}^{2}}}{S_{0}}, \\ P_{C} = \frac{\sqrt{S_{3}^{2}}}{S_{0}}, \\ \theta = \frac{\arctan\left(\frac{S_{1}}{S_{2}}\right)}{2}. \end{cases}$$
 (1)

Generally, the Muller matrix and Stokes parameters are used to characterize the effect of an optical component on the polarization state. The Muller matrix is only related to the optical parameters of the component, and the basic form is shown in the following equations:

$$\begin{bmatrix} S_0 \\ S_1 \\ S_2 \\ S_3 \end{bmatrix}_{out} = R(-\alpha) \cdot \begin{bmatrix} 1 & -\cos 2\varphi & 0 & 0 \\ -\cos 2\varphi & 1 & 0 & 0 \\ 0 & 0 & \sin 2\varphi \cos \delta & \sin 2\varphi \sin \delta \\ 0 & 0 & -\sin 2\varphi \sin \delta & \sin 2\varphi \cos \delta \end{bmatrix} \cdot R(\alpha) \begin{bmatrix} S_0 \\ S_1 \\ S_2 \\ S_3 \end{bmatrix}_{in},$$
 (2)

TABLE I. Refractive index data of common coating materials at 10.2 eV.

Material	Refractive index	
Au Ni Pt Ru	1.268 + 0.972j 0.948 + 0.834j 1.344 + 1.178j 0.900 + 0.770j	

$$\begin{cases} \varphi = \arctan\left(\frac{r_p}{r_s}\right), \\ \delta = \delta_p - \delta_s. \end{cases}$$
 (3)

Here,  $R(\alpha)$  is the transformation matrix between the laboratory coordinate system and the polarizer coordinate system,  $r_p$ ,  $r_s$  are the reflections in the S and P-directions, and  $\delta_p$ ,  $\delta_s$  are the phase shifts in the S and P-directions. All of the above-mentioned parameters can be acquired from the optical parameter database. <sup>22,23</sup> Therefore, polarization diagnostics are performed by rotating the polarizer and fitting the curve of the output intensity as a function of the polarizer angle, thereby obtaining the Stokes parameters and polarization state information

The reflection polarization technique is based on the principle of Brewster angle polarization to separate and detect the polarization component using the difference in reflectivity between S- and P-direction polarization components. To ensure accurate polarization measurements, the polarizer must exhibit a high extinction ratio  $\left(\frac{R_s}{R_0}\right)$ . It is highest at the Brewster angle after the incident

light reflects off a mirror surface.<sup>24</sup> In the DCLS wavelength range (50–150 nm), the extinction ratio of the commonly used metal coatings (Au/Ni/Pt/Ru) in free-electron laser beamlines is less than 10 after one reflection. It is not enough to diagnose the polarization purity within 95%. Multilayer coatings exhibit high extinction ratios only within narrow wavelength bands; therefore, a single mirror cannot cover the full wavelength range. Therefore, multiple reflections with a single metal coating have to be used to increase the extinction ratio to at least 100, and the incident outgoing light can be coaxial so that the detector does not need to rotate with the polarizer. In order to have good performance in the full wavelength range, incident angle, coating, and how many mirrors are considered carefully.

The incident angle was optimized at the Brewster angle of  $121.6\,\mathrm{nm}\,(10.2\,\mathrm{eV})$ , which is the most commonly used wavelength of the end-station in DCLS. <sup>25,26</sup> Table I summarizes the refractive index data of four materials, Au, Ni, Ru, and Pt, according to the optical properties database, <sup>22,23</sup> and the extinction ratio for the coating materials shown in Fig. 2(a) is calculated based on the data in Table I. Obviously, the Au-coated film is the good choice for  $121.6\,\mathrm{nm}$  at the Brewster angle of  $59.6^\circ$ . While one mirror is not enough, it is worth it to add more mirrors to increase the extinction ratio. From Fig. 2(b), it can be seen that after four reflections, the extinction ratio of the polarizer ranges from 100 to 1400 due to different wavelengths. This means that the diagnostic precision for the degree of polarization is better than 1%, which meets the diagnostic accuracy requirements. The Au-coated four-mirror polarizer with the incidence angle of  $59.6^\circ$  is chosen for the VUV polarimeter.

Furthermore, from Eq. (2), one can derive the relationship between the output light intensity, the azimuth of the four-reflection polarizer, and the Stokes parameters of the incident light,

$$I = S_{0out} = \left(\frac{R_S + R_P}{2}\right)^4 \begin{cases} S_0(\cos 2\varphi(2\cos 2\varphi + \cos 2\varphi(\cos^2 2\varphi + 1)) + 3\cos^2 2\varphi + 1) \\ -S_1\cos 2\alpha(2\cos 2\varphi + \cos 2\varphi(\cos^2 2\varphi + 1) + \cos 2\varphi(3\cos^2 2\varphi + 1)) \\ -S_2\sin 2\alpha(2\cos 2\varphi + \cos 2\varphi(\cos^2 2\varphi + 1) + \cos 2\varphi(3\cos^2 2\varphi + 1)) \end{cases}, \tag{4}$$

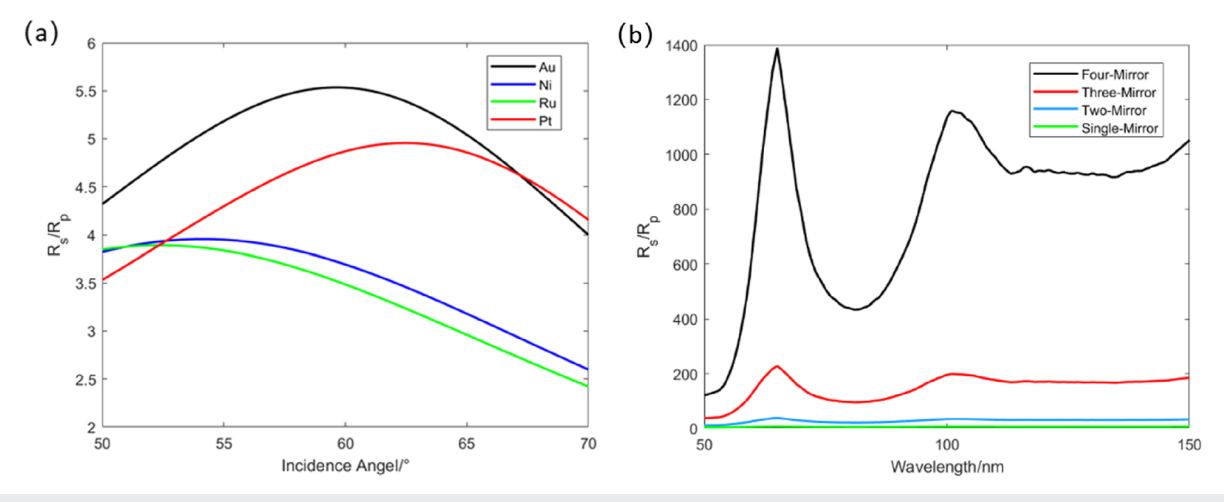


FIG. 2. (a) Extinction ratio of the polarizer with different coating materials at different incident angles at 121.6 nm. (b) Extinction ratio of Au-coated polarizers with different numbers of mirrors at an incident angle of 59.6° in the 50–150 nm range.

where  $\alpha$  is the azimuth of the polarizer. The polarization state can be obtained by fitting the relationship between the azimuth angle of the polarizer and the light intensity detected by the Microchannel Plate (MCP) detector.

# B. Mechanical design

The overall mechanical design of the device is shown in Fig. 3, which consists of rotation, detection, and alignment systems.

Polarization diagnosis needs to detect the light intensity passing through the polarizer at different rotation angles. A four Au coating mirror reflection system is installed on an RSX3K6-LS high-precision polarizer rotation stage manufactured by Arun Microelectronics Corporation with the moving range of  $0^{\circ}$ –360° and the precision of  $0.1^{\circ}$  to ensure accurate measurement of the linear polarization angle. The substrate of the Au coating mirror is single crystal silicon, the coating thickness is 100 nm, the roughness is about 0.2 nm, and the overall length, width, and thickness of the mirror are  $30\times20\times10$  mm. The polarizer and rotary stage are mounted on a linear displacement stage, enabling their insertion and retraction from the optical path.

After four times reflection, the light intensity will only retain about 3.11% ( $Rs \approx 0.42$ ). To measure the light intensity accurately in a relatively large dynamics range, which is the key to obtaining high polarization purity, two types of detectors are used, photodiodes (PD) for high light intensities and MCP for low light intensities. This experiment was conducted under weak light conditions, with the incident light intensity ~2  $\mu$ J, measured using the SXUV100 photodiode manufactured by Opto-Diode Corporation. We select a MCP made by Northern Night Vision Technology Corporation and a self-designed metal shell to assemble the MCP detector for low light intensity detection. The MCP detector maintains a dynamic range with linearity over three orders of magnitude, which can ensure that

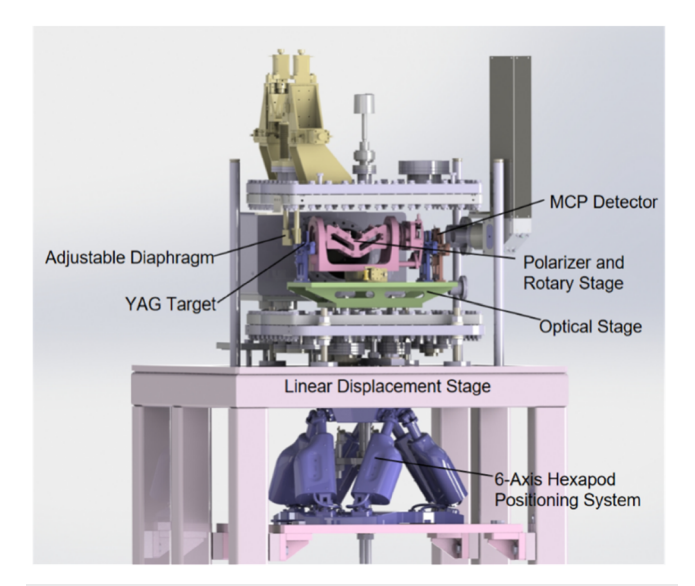


**FIG. 3.** Mechanical schematics of the optical polarimeter on the six-axis hexapod positioning system.

the signal will not be distorted by the change of light intensity caused by the rotating polarizer.

In addition, Yttrium Aluminum Garnet (YAG) scintillator targets and the BrevaST six-axis hexapod positioning system, manufactured by Symetre Corporation, facilitate the precise online collimation of the optical polarimeter by adjusting its attitude to make sure that the FEL accurately traverses the centers of the YAG scintillator targets located both in front of and behind the polarizer. Furthermore, as the DCLS-FEL2 has four branches, all components are mounted on the hexapod positioning system, which allows for precise and rapid adjustment of the system after deployment. Due to the strong absorption of VUV radiation in the atmosphere, the components of the polarimeter are encased within an ultra-high vacuum chamber, maintaining the vacuum level of  $5\times 10^{-7}$  Pa.

#### **III. EXPERIMENTAL RESULTS**

# A. Polarization diagnostic results at DCLS-FEL2

Polarization diagnostic experiments were conducted at the DCLS-FEL2 beamline. The pulse energy of the FEL during the experiment was 2  $\mu$ J/pulse, detected by the SXUV100 photodiode from Opto-Diode Corporation. The central wavelength was adjusted to 121.6 nm, as measured by the online spectrometer. Owing to multiple reflections of the polarizer, the light intensity is very weak when it reaches the MCP detector. The MCP detector can amplify electronic signals through two microchannels, facilitating the detection of weak signals. In addition, the U5309A acquisition card, manufactured by Acqiris Corporation, was used to collect the intensity signal from the MCP detector.

Light intensity passing through the polarizer was collected at different polarizer azimuths. Figure 4(a) shows the variation of light intensity measured by the MCP detector with the azimuth angle of the polarizer and the fitting results in both linear and circular polarization modes. The scanning step of the azimuth angle is  $10^{\circ}$ , and the measured results fit well with the curve calculated from Formula (4). In addition, a diagram of the electric vector oscillation mode reconstructed from the experimental data was plotted in Fig. 4(b).

Multiple tests were conducted at DCLS-FEL2, and the diagnostic results are shown in Tables II and III.

Tables II and III show the test results of linear polarization degree  $P_L$ , circular polarization degree  $P_C$ , polarization angle  $\theta$ , and Stokes parameter  $\begin{bmatrix} S_0 & S_1 & S_2 & S_3 \end{bmatrix}$ , as well as their average values and standard deviations. The results show that the linear polarization angle is measured with an accuracy of  $\pm 1^\circ$ , and the linear and circular polarization degree is about 95%.

The measured polarization state shows a slight deviation from the theoretically perfect polarization. Theoretically, horizontally polarized light is not affected by distortions introduced by the M1M2 transmission. Hence, the measurement errors mainly arise from light intensity fluctuations and the variation in the MCP detector's quantum efficiency with intensity. To further demonstrate the impact of these two error sources on the results, a simulation was performed under horizontally polarized conditions. During the measurements, the standard deviation (STD) of the light intensity fluctuations was ~20%, and it was assumed that the MCP experiences about a 3% efficiency drop due to saturation<sup>28</sup> when obtaining close to the light intensity peak. Nine simulations were conducted, and the linear polarization degree and polarization angle were

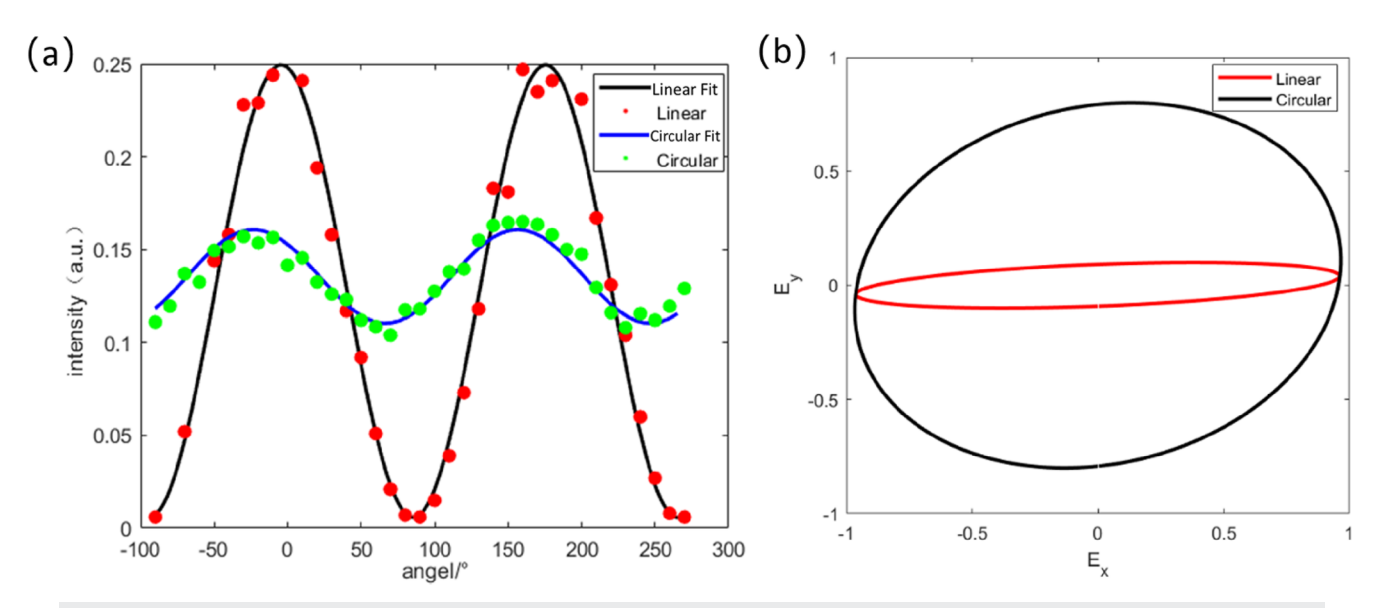


FIG. 4. (a) Curve of light intensity varies with the polarizer azimuth angle and the fitting results. (b) Electric vector vibration mode of linear and circular polarization.

**TABLE II.** Linear polarization diagnostic results.

TN	$P_L$	θ	$S_1/S_0$	$S_2/S_0$	S <sub>3</sub> /S <sub>0</sub>	$R^2$
1	0.944	-3.56	0.936	-0.117	0.331	0.993
2	0.935	-2.58	0.931	-0.084	0.356	0.988
3	0.940	-3.32	0.933	-0.109	0.342	0.987
4	0.982	-2.61	0.978	-0.089	0.190	0.996
5	0.937	-4.43	0.926	-0.144	0.349	0.932
6	0.953	-4.58	0.941	-0.152	0.302	0.970
7	0.920	-1.84	0.918	-0.059	0.391	0.984
8	0.930	-3.39	0.923	-0.110	0.369	0.972
9	0.955	-4.45	0.943	-0.148	0.297	0.959
$Mean \pm STD$	$0.944 \pm 0.018$	$-3.418 \pm 0.956$	$0.937 \pm 0.017$	$-0.112 \pm 0.032$	$0.325 \pm 0.059$	

**TABLE III.** Circular polarization diagnostic results.

TN	$P_C$	θ	$S_1/S_0$	$S_2/S_0$	$S_3/S_0$	$R^2$
1	0.9238	-24.370	-0.2525	-0.2878	0.9238	0.935
2	0.9390	-22.410	-0.2439	-0.2424	0.9390	0.944
3	0.9725	-19.350	-0.1818	-0.1456	0.9725	0.935
4	0.9329	-20.110	-0.2750	-0.2325	0.9329	0.960
5	0.9825	-23.390	-0.1276	-0.1357	0.9825	0.915
6	0.9649	-27.060	-0.1539	-0.2128	0.9649	0.948
7	0.9089	-22.040	-0.2996	-0.2901	0.9089	0.948
8	0.9347	-25.160	-0.2269	-0.2736	0.9347	0.956
9	0.9734	-20.430	-0.1733	-0.1499	0.9734	0.992
$Mean \pm STD$	$0.948 \pm 0.026$	$-22.702 \pm 2.548$	$-0.215 \pm 0.058$	$-0.219 \pm 0.062$	$0.948 \pm 0.026$	

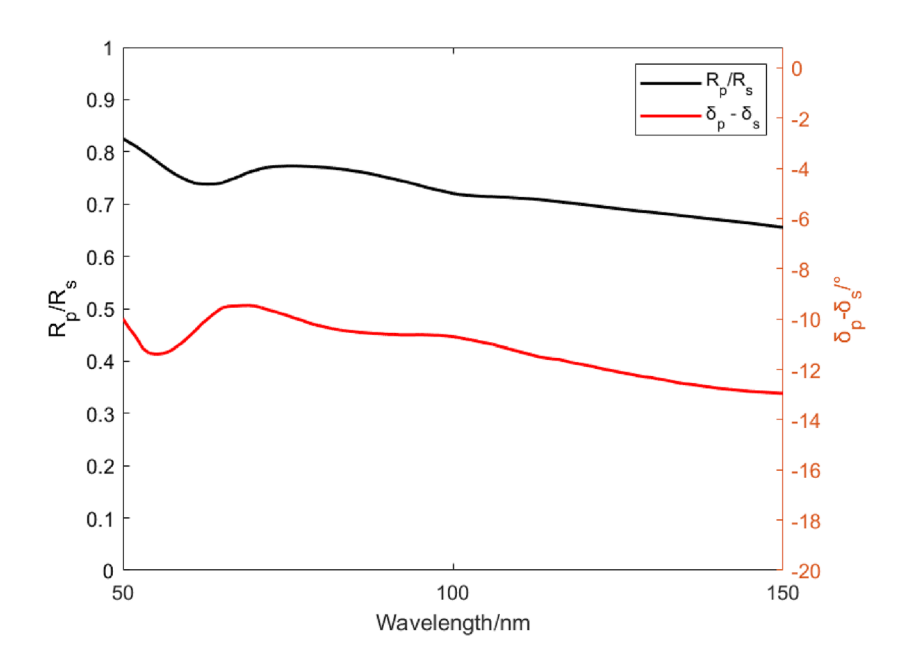


FIG. 5. Reflectivity ratio and phase difference induced by the FEL2 beamline transmission over the full wavelength range of DCLS.

statistically analyzed, yielding the results shown in the following formula:

$$\begin{cases} P_{L-Simulation} = 0.9531 \pm 0.0183, \\ \theta_{Simulation} = -0.74^{\circ} \pm 1.24^{\circ}. \end{cases}$$
 (5)

The above-mentioned results are very close to the measured results shown in Table II, providing a robust explanation for the observed error sources.

# B. Calibration results of beamline transmission matrix

The DCLS-FEL2 beamline comprises two beamline optic elements, M1 and M2, with Au coated film and a 2.5° grazing angle. The schematic diagram of the beamline and optical polarimeter was shown in Fig. 1.

The above beamline transmission system will introduce transmission distortion in the polarization state during the reflection process, which is due to the distortion caused by the additional phase difference and the difference in reflectivity of S- and P-directions introduced by each mirror. As shown in Fig. 5, we calculated the

reflectivity ratio for P- and S-directions and the induced phase difference from the two mirrors of DCLS-FEL2 based on the optical parameter database.  $^{22,23}$  The results indicate that after transmission, the reflectivity ratio is  $\sim\!0.70$  and the phase difference is about  $-12^\circ$ . This has a non-negligible impact on the transmission of the polarization state, and the effect will be further amplified when more mirrors are involved.

DCLS-FEL2 is fully employed with a EPU; therefore, when the EPU operates in circular polarization mode, the polarization state of the FEL should theoretically be 100% circularly polarized. Based on this, we employed polarization diagnostic data obtained in the circular polarization mode to calibrate the beamline transmission distortion in DCLS-FEL2. The circular polarization diagnostic results recorded in Table III are the outcomes of fully circularly polarized light after beamline distortion. Therefore, by substituting  $S_{in} = [1, 0, 0, 1]$ ,  $S_{out} = [1, -0.215, -0.219, 0.948]$ , and  $\alpha = 0$  into Formula (2), the transmission matrix of DCLS-FEL2 can be solved. The transmission matrix calibration results for the DCLS-FEL2 beamline.

$$M_{DCLS-FEL2} = \begin{bmatrix} 1 & -0.215 \pm 0.058 & 0 & 0 \\ -0.215 \pm 0.058 & 1 & 0 & 0 \\ 0 & 0 & 0.948 \pm 0.026 & -0.219 \pm 0.062 \\ 0 & 0 & 0.219 \pm 0.062 & 0.948 \pm 0.026 \end{bmatrix}.$$
(6)

In order to validate the measured transmission matrix of the DCLS-FEL2, we calculated the theoretical transmission matrix of the DCLS-FEL2 using the expression of the Muller matrix in Formula (2), according to the refractive index of Au recorded in Table I,

$$M_{Theory} = \begin{bmatrix} 1 & -\cos 2\varphi & 0 & 0 \\ -\cos 2\varphi & 1 & 0 & 0 \\ 0 & 0 & \sin 2\varphi \cos \delta & \sin 2\varphi \sin \delta \\ 0 & 0 & -\sin 2\varphi \sin \delta & \sin 2\varphi \cos \delta \end{bmatrix} = \begin{bmatrix} 1 & -0.179 & 0 & 0 \\ -0.179 & 1 & 0 & 0 \\ 0 & 0 & 0.963 & -0.203 \\ 0 & 0 & 0.203 & 0.963 \end{bmatrix}.$$
(7)

It is evident that the theoretical transmission matrix in Formula (7) falls within the STD of the measured results in Formula (6), demonstrating agreement between theory and experiment. This strong correlation validates the feasibility of our method for calibrating the beamline's transmission matrix. This provides strong support for compensating for the distortion of the polarization state at the end-station.

From the above-mentioned analysis, it is clear that the deviation between the mean measured values in Table III and those of ideal circularly polarized light originates from transmission distortions of the polarization state. Meanwhile, the STD observed in the measurements is primarily due to a 20% fluctuation in light intensity. To demonstrate this point, the measurement errors of the polarization state under a 20% intensity fluctuation were simulated, as shown in the following formula:

$$\begin{cases} P_{C-Simulation} = 0.9487 \pm 0.0201, \\ \theta_{Simulation} = -22.15^{\circ} \pm 2.94^{\circ}. \end{cases}$$
 (8)

The simulation results are in good agreement with the measured data in Table III, providing a robust explanation for the observed error sources.

# IV. CONCLUSION

Polarization diagnostics are essential for the advancement of photon science. Using the extinction technique based on the Brewster angle reflection principle, we have developed a polarization diagnostic device capable of high-precision polarization diagnosis and rapid deployment on the VUV-FEL facility. A linear polarization angle precision of  $\pm 1^{\circ}$  and a polarization degree of 95% were experimentally validated. This provides critical data support for the experiments requiring polarized light, such as surface-catalyzed reactions and magnetic/chiral material detection. The device is located on the DCLS-FEL2 beamline. It is routinely used and can be easily deployed to different branch lines. Calibration of the DCLS-FEL2 beamline transmission matrix has also been achieved through circular polarization diagnostic results, providing an essential dataset for polarization distortion compensation at downstream end-stations.

# **ACKNOWLEDGMENTS**

This work was financially supported by the Shenzhen Science and Technology Program (Grant No. RCBS20221008093327057), the National Key R&D Program of China (Grant No. 2018YFE0203000), the National Natural Science Foundation of China (Grant Nos. 22303055, 22288201, and 22203091), the Scientific Instrument Developing Project of the Chinese Academy of Sciences (Grant No. GJJSTD20190002), the Strategic Priority

Research Program of the Chinese Academy of Sciences (Grant Nos. XBD0970000 and XBD0970100), and the Liaoning Science and Technology Plan Project (Grant No. 2023JH1/11000001). We acknowledge the staff members of the Dalian Coherent Light Source (https://cstr.cn/31127.02.DCLS) for providing technical support and assistance in data collection and analysis.

#### **AUTHOR DECLARATIONS**

#### Conflict of Interest

The authors have no conflicts to disclose.

#### **Author Contributions**

Mingchang Wang: Conceptualization (equal); Data curation (equal); Formal analysis (equal); Investigation (equal); Methodology (equal); Writing - original draft (equal). Bingbing Zhang: Data curation (equal); Validation (equal). Siyuan Tan: Data curation (equal); Resources (equal). Zhixiang Wen: Resources (equal); Software (equal). Jinxin Wang: Data curation (equal); Resources (equal). Long Huang: Data curation (equal); Resources (equal). Baoning Sun: Data curation (equal); Resources (equal). Zequn Wang: Data curation (equal); Resources (equal). Jitao Sun: Data curation (equal); Resources (equal). Xinmeng Li: Data curation (equal); Resources (equal). Jiayue Yang: Data curation (equal); Resources (equal). Qinming Li: Conceptualization (equal); Data curation (equal); Methodology (equal); Resources (equal); Supervision (equal); Validation (equal); Writing - review & editing (equal). Weiqing Zhang: Conceptualization (equal); Funding acquisition (equal); Methodology (equal); Project administration (equal); Resources (equal); Supervision (equal); Writing - review & editing (equal).

#### **DATA AVAILABILITY**

The data that support findings of this study are available from the corresponding authors upon reasonable request.

# **REFERENCES**

<sup>1</sup>P. G. O'Shea and H. P. Freund, Science **292**(5523), 1853–1858 (2001).

<sup>2</sup>Q. Li, Y. Yu, J. Yang, H. Ding, L. Shi, K. Tao, G. Wang, G. Wu, D. Dai, and W. Zhang, Proc. SPIE 11038, 1103812 (2019).

<sup>3</sup>Y. Yu, Q. Li, J. Yang et al., Chin. J. Lasers **46**(1), 0100005 (2019).

<sup>4</sup>J. Sun, X. Li, J. Yang et al., Nucl. Instrum. Methods Phys. Res., Sect. A **1063**, 169320 (2024).

<sup>5</sup>C. Spezzani, E. Allaria, M. Coreno, B. Diviacco, E. Ferrari, G. Geloni, E. Karantzoulis, B. Mahieu, M. Vento, and G. De Ninno, Phys. Rev. Lett. **107**(8), 084801 (2011).

- <sup>6</sup>C. S. Hwang and S. Yeh, Nucl. Instrum. Methods Phys. Res., Sect. A **420**(1-2), 29–38 (1999).
- <sup>7</sup>G. Hartmann, A. O. Lindahl, A. Knie, N. Hartmann, A. A. Lutman, J. P. MacArthur, I. Shevchuk, J. Buck, A. Galler, J. M. Glownia *et al.*, Rev. Sci. Instrum. **87**(8), 083113 (2016).
- <sup>8</sup>D. Faccialà, M. Devetta, S. Beauvarlet, N. Besley, F. Calegari, C. Callegari, D. Catone, E. Cinquanta, A. Ciriolo, and L. Colaizzi, Phys. Rev. X 13(1), 011044 (2023)
- <sup>9</sup>M. Ilchen, P. Schmidt, N. M. Novikovskiy, G. Hartmann, P. Rupprecht, R. N. Coffee, A. Ehresmann, A. Galler, N. Hartmann, W. Helml *et al.*, Commun. Chem. 4(1), 119 (2021).
- <sup>10</sup>N. Kerber, D. Ksenzov, F. Freimuth, F. Capotondi, E. Pedersoli, I. Lopez-Quintas, B. Seng, J. Cramer, K. Litzius, D. Lacour *et al.*, Nat. Commun. 11(1), 6304 (2020).
- <sup>11</sup>O. Bünermann, H. Jiang, Y. Dorenkamp, D. J. Auerbach, and A. M. Wodtke, Rev. Sci. Instrum. 89(9), 094101 (2018).
- <sup>12</sup>O. Bünermann, A. Kandratsenka, and A. M. Wodtke, J. Phys. Chem. A **125**(15), 3059–3076 (2021).
- <sup>13</sup> R. M. Kim, J.-H. Huh, S. Yoo, T. G. Kim, C. Kim, H. Kim, J. H. Han, N. H. Cho, Y.-C. Lim, S. W. Im *et al.*, Nature **612**(7940), 470–476 (2022).
- <sup>14</sup>P. Gerbier, N. Domingo, J. Gómez-Segura, D. Ruiz-Molina, D. B. Amabilino, J. Tejada, B. E. Williamson, and J. Veciana, J. Mater. Chem. 14(15), 2455–2460 (2004).
- <sup>15</sup>T. Kihara, Appl. Mech. Mater. **3**, 235–242 (2005).
- <sup>16</sup>W. Grizolli, J. Laksman, F. Hennies, B. N. Jensen, R. Nyholm, and R. Sankari, Rev. Sci. Instrum. 87(2), 025102 (2016).

- <sup>17</sup>H. Wang, S. S. Dhesi, F. Maccherozzi, S. Cavill, E. Shepherd, F. Yuan, R. Deshmukh, S. Scott, G. van der Laan, and K. J. S. Sawhney, Rev. Sci. Instrum. 82(12), 123301 (2011).
- <sup>18</sup>E. Roussel, E. Allaria, C. Callegari, M. Coreno, R. Cucini, S. Di Mitri, B. Diviacco, E. Ferrari, P. Finetti, D. Gauthier et al., Photonics 4(2), 29 (2017).
- <sup>19</sup>E. Ferrari, E. Allaria, J. Buck, G. De Ninno, B. Diviacco, D. Gauthier, L. Giannessi, L. Glaser, Z. Huang, M. Ilchen *et al.*, Sci. Rep. 5(1), 13531 (2015).
- <sup>20</sup>C. Latimer, M. MacDonald, and P. Finetti, J. Electron Spectrosc. Relat. Phenom. **101**, 875–878 (1999).
- <sup>21</sup> Q. Zhang, B. Deng, Y. Chen, B. Liu, S. Chen, J. Fan et al., J. Instrum. 12(10), T10003 (2017).
- <sup>22</sup>E. D. Palik, *Handbook of Optical Constants of Solids* (Academic Press, 1998).
- <sup>23</sup>D. Smith, E. Shiles, M. Inokuti, and E. Palik, *Handbook of Optical Constants of Solids 1* (Academic Press, 1985).
- <sup>24</sup>P. J. Ouseph, K. Driver, and J. Conklin, Am. J. Phys. 69(11), 1166–1168 (2001).
- <sup>25</sup>S. An, S. Ranjan, K. Yuan, X. Yang, and R. T. Skodje, Phys. Chem. Chem. Phys. 23(15), 9235–9248 (2021).
- <sup>26</sup>Y. Chang, M. N. R. Ashfold, K. Yuan, and X. Yang, Natl. Sci. Rev. 10(8), nwad158 (2023).
- <sup>27</sup> M. Wang, Y. Yu, J. Yang, Q. Li, and W. Zhang, Rev. Sci. Instrum. 95(6), 063101 (2024).
- <sup>28</sup>O. L. Landen, P. M. Bell, J. A. Oertel, J. J. Satariano, and D. K. Bradley, Proc. SPIE **2002**, 2–13 (1993).